UNCLASSIFIED

~~CONFIDENTIAL~~

NACA

RESEARCH MEMORANDUM

TRANSONIC FLIGHT TESTS TO COMPARE THE ZERO-LIFT DRAG

OF UNDERSLUNG AND SYMMETRICAL NACELLES VARIED

CHORDWISE AT 40 PERCENT SEMISPAN OF

A 45° SWEPTBACK, TAPERED WING

By William B. Pepper, Jr., and Sherwood Hoffman

Langley Aeronautical Laboratory
Langley Air Force Base, Va.

JPL LIBRARY

CALIFORNIA INSTITUTE OF TECHNOLOGY

NATIONAL ADVISORY COMMITTEE
FOR AERONAUTICS
WASHINGTON
October 25, 1950

~~CONFIDENTIAL~~

UNCLASSIFIED

CONFIDENTIAL

NATIONAL ADVISORY COMMITTEE FOR AERONAUTICS

RESEARCH MEMORANDUM

TRANSONIC FLIGHT TESTS TO COMPARE THE ZERO-LIFT DRAG

OF UNDERSLUNG AND SYMMETRICAL NACELLES VARIED

CHORDWISE AT 40 PERCENT SEMISPAN OF

A 45° SWEPTBACK, TAPERED WING

By William B. Pepper, Jr., and Sherwood Hoffman

SUMMARY

Rocket-powered models were flown at transonic speeds to determine the effect of nacelle location on the zero-lift drag. Nacelles of fineness ratio 9.66 were mounted in underslung and symmetrical (midwing) positions along the wing chord at 40 percent of the semispan. The noses of the nacelles were located at four chordwise stations equivalent to 0.35, 0.50, 0.76, and 1.20 wing chords ahead of the wing leading edge at 40 percent wing semispan. The wing had a sweepback angle of 45° along the quarter-chord line, an aspect ratio of 6.0, a taper ratio equal to 0.6, and an NACA 65A009 airfoil section in the free-stream direction. The fuselage fineness ratio was 10.0.

Results from flight tests showed that no unfavorable interference effects were evident for either underslung or symmetrical nacelle positions at Mach numbers between 0.80 and 0.93. At a Mach number of 1.0 large unfavorable interference effects were present and caused the experimental nacelle drag coefficients to be from 85 percent to 285 percent higher than the value estimated for the nacelle without interference. Nacelles mounted symmetrically on the wing generally had lower drag coefficients than nacelles located in underslung positions at Mach numbers from 0.95 to 1.20. The symmetrically mounted nacelles located in rear positions at the 35- and 50-percent-chord positions gave the lowest drag, and the underslung location at the 76-percent-chord location had the highest drag. The addition of nacelles to the wings of the models, independent of their chordwise location at 40 percent of the semispan, reduced the Mach number at which the transonic drag rise of the total configuration occurred by 0.03 to 0.07.

INTRODUCTION

As part of a general transonic research program of the National
Advisory Committee for Aeronautics to determine the aerodynamic proper-
ties of promising configurations, rocket-propelled models were tested
in free flight to determine the variations of zero-lift drag coefficient
for a medium-size bomber configuration with nacelles in various posi-
tions on the wings.

Up to the present time investigations of wing-body-nacelle inter-
ference at transonic speeds have been confined to fighter models with
low-aspect-ratio wings. Subsonic data on wing-body-nacelle interference
effects are available for both low- and high-aspect-ratio-wing aircraft;
however, there is a lack of information for medium bomber configurations
with high-aspect-ratio wings throughout the transonic speed range.

In order to carry out this investigation a wing-body test configu-
ration with a low drag coefficient and a high force break Mach number
well above 0.9 was desired. The wing selected, having a sweepback angle
of 45° and an aspect ratio of 6, appears promising for high-speed bomber
applications. A thickness ratio of 9 percent was believed adequate to
insure that the wing would be structurally applicable to a high-speed
bomber and also maintain a force break Mach number above 0.9.

A suitable low-drag fuselage was based on the transonic fuselage
developed in free-fall tests by the NACA. This body has low subsonic
drag and a force break Mach number above 0.9.

The nacelles adopted for the investigation were designed to house
an axial-flow turbojet with thrust augmentation by afterburning. This
space requirement results in a nacelle having a fineness ratio which is
compatible with low drag. Since the primary purpose of the first phase
of this investigation is to explore various chordwise locations for
symmetrical and underslung wing nacelles, it was desired to simplify
the tests by conducting the present investigation without air flow
through the nacelles. Accordingly, a nose fairing was adapted which
fairs the air inlet of the nacelle to a pointed nose, making it a solid
nacelle. However, the basic lines of the nose are designed to accommodate
NACA 1-series inlets with critical Mach numbers above M = 0.9.

Tests of the resulting configuration yielded curves of drag-
coefficient variations for models with and without nacelles, nacelle-
plus-interference drag coefficients for various nacelle locations, and
nacelle base-drag and base-pressure variations over a continuous Mach
number range of M = 0.8 to M = 1.25. The Reynolds number range of the
tests is comparable to that of a full-scale bomber flying at 60,000 feet.

SYMBOLS

A   aspect ratio $\left(b^2/S_W\right)$

a   longitudinal acceleration, feet per second per second

b   wing span, feet

C_D total drag coefficient, based on S_W

C_{D_B} nacelle base-pressure drag coefficient, based on S_F

C_{D_N} drag coefficient for nacelle plus interference, based on S_F

C_{p_B} base-pressure coefficient $\left(\dfrac{p_B - p}{q}\right)$

c   wing chord at the 40-percent station, inches

e   distance between wing leading edge and nacelle inlet, inches

g   acceleration due to gravity, 32.2 feet per second per second

M   Mach number $\left(V/V_S\right)$

p   free-stream static pressure, pounds per square foot

p_B nacelle base pressure, pounds per square foot

q   free-stream dynamic pressure, pounds per square foot $\left(\dfrac{\gamma}{2}\, pM^2\right)$

R   Reynolds number per foot

S_B nacelle base area, square feet

S_F frontal area of one nacelle, square feet

S_W total wing plan-form area, square feet

V   velocity along flight path, feet per second

V_S speed of sound, feet per second

W   model weight after burnout, pounds

γ ratio of specific heats, 1.4 for air; or flight-path
             angle

x   station, inches

y   ordinate, inches

MODELS

Details and dimensions of the wing-body-fin combination, the solid nacelle, and the nacelle reference body are given in figures 1 and 2 and tables I to III. Photographs showing the general arrangements of the models flown are presented as figure 3.

The transonic fuselage, described in reference 1, was reduced from a fineness ratio of 12 to 10 by cutting off the rear one-sixth of the body. In order to fit a 3.25-inch Mk. 7 aircraft rocket motor into this body, the rear 28 percent of the modified body was enlarged. The fuselage was constructed from wood and had an aluminum nose. The frontal area of the fuselage was equal to 0.242 square foot.

The leading edge of the wing intersected the fuselage at the maximum diameter. This wing had a sweepback angle of $45°$ along the quarter-chord line, an aspect ratio of 6.0 based on total wing area of 3.878 square feet (including area in the body), a taper ratio equal to 0.6, and an NACA 65A009 airfoil section in the free-stream direction. This wing configuration was the same as that used in reference 2. The ratio of total wing plan-form area to the fuselage frontal area was 16.0. Sheet steel inlays, 0.04 inch thick, were imbedded near the upper and lower surfaces of the wooden wing. The steel strengthened the wing and served as an antenna for the NACA two-channel radio telemeter.

The nacelles were bodies of revolution constructed of wood having a fineness ratio of 9.66 and a frontal area of 0.034 square foot. Each nacelle used for this investigation was designed to have an NACA 1-50-250 nose-inlet profile (based on data in reference 3), a cylindrical mid-section, and an afterbody of NACA 111 proportions (reference 4). For the present investigation a conical lofted nose plug (reference 5) was used to close off the nacelle inlet. The dimensioning system used to define the chordwise location of the nacelles refers to the distance

of the nacelle inlet ahead of the wing leading edge at the 40-percent-semispan-wing station. The chordwise locations expressed in percent of wing chord were 35, 50, 76, and 120 percent.

Two vertical positions were tested. The symmetrical or midwing position had the nacelle center line in the wing plane. For the underslung positions (fig. 3(c)), the nacelle center lines remained parallel to the wing chord plane and were displaced on opposite sides of the wing plane. This asymmetric arrangement was used so that any trim change would produce roll and the model would fly at essentially zero lift. Tracking photographs of the models in flight, however, revealed no significant roll or pitch.

Cross-sectional views of the nacelle and of the wing-nacelle intersection taken through the nacelle center line are shown in figures 2(a) and 2(b). No filleting was employed at the nacelle-wing juncture.

Two vertical aluminum fins were used to stabilize the model directionally. No fins were required in the horizontal plane because the sweptback wing was located far enough rearward on the fuselage to stabilize the model in this plane (fig. 1). The leading edges of the fins were swept back 45° and the fins were 0.091 inch thick. The exposed fin plan-form area for two fins equaled 0.468 square foot.

TESTS AND MEASUREMENTS

Ten rocket-propelled zero-lift models were tested at the Langley Pilotless Aircraft Research Station, Wallops Island, Va. Three identical models without nacelles were flown to find the basic drag of the wing-body-fin combination as accurately as possible and the scatter of experimental values that would exist for subsequent models. On the remaining seven models, underslung and symmetrically mounted nacelles were varied along the chord at 40 percent of the wing semispan. These models are classified according to nacelle position in figure 2.

Each model was propelled by a two-stage rocket system and launched from a rail launcher (fig. 3(a)). The first stage consisted of a 5-inch, lightweight, high-velocity aircraft rocket motor that served to accelerate the model from zero velocity to high subsonic speeds. For the second stage, a 3.25-inch Mk. 7 aircraft rocket motor was installed in the fuselage to accelerate the model to supersonic speeds. Tracking instrumentation consisting of a CW Doppler velocimeter and an NACA modified SCR584 tracking unit was used to determine the flight path and deceleration during the coasting flight. A survey of atmospheric conditions at the time of each launching was made through radiosonde measurements from

an ascending balloon. ·Nacelle base-pressure variations for model J
were obtained through an orifice 3/16 inch in diameter located at the
center of the base and by use of the NACA telemetering system.

The values of drag·coefficient, based on total wing plan-form area
for each model, were calculated for flight conditions by use of the
formula

$$C_D = -\frac{W}{qg S_W} (a + g \sin \gamma)$$

The difference in drag coefficients of models with nacelles and without
nacelles is defined as nacelle-plus-interference drag. This coefficient,
based on nacelle frontal area, is

$$C_{D_N} = \left(C_{D_{nacelles\ on}} - C_{D_{nacelles\ off}} \right) \frac{S_W}{2 S_F}$$

Base pressures were converted to base drag coefficients, based on
nacelle frontal area, through the relation

$$C_{D_B} = \frac{\left(p_B - p \right)}{q} \frac{S_B}{S_F}$$

The Mach number was determined from the velocity of each model and
the speed of sound at altitude from corresponding radiosonde records.

RESULTS AND DISCUSSION

Flight tests of the models covered a Reynolds number range from
4.6×10^6 per foot at $M = 0.8$ to 9.3×10^6 per foot at $M = 1.3$, as
shown in figure 4. Drag coefficients obtained from the tests are shown
in figures 5 to 7. These figures permit a comparison of total drag,
nacelle-plus-interference drag, and interference drag coefficients for
the various nacelle positions at zero lift.

The nacelle-plus-interference drag coefficient C_{D_N} is obtained by
taking the difference in drag of models with and without nacelles. Since
this drag results from the subtraction of two relatively large values, a
large error could be encountered. Therefore, three models without nacelles
were flown to determine the scatter in the data for identical models. The
faired curves for the three models, based on total wing plan-form area

of 3.878 square feet, are shown in figure 5 and are compared in order to determine the experimental error in the test results. The deviation of the faired curves indicates that the errors to be expected are of the order of ±0.0004. From this value, the errors in the nacelle-plus-interference drag coefficients would be expected to be ±0.023 (based on nacelle frontal area). Photographs of the models in flight showed that there was no appreciable roll due to the underslung nacelle locations.

Curves showing the variation of total drag and nacelle-plus-interference drag for the models through the test Mach number range are given for symmetrical nacelles in figures 6(a) to 6(d) and for under-slung nacelles in figures 6(e) to 6(g). The curve for the model with nacelles off is the average of the faired curves in figure 5. The nacelle-plus-interference drag is compared with the drag of a body of revolution having the same fineness ratio and a shape similar to that of the nacelle. The drag of this body is referred to as the drag of an isolated nacelle or an unmounted nacelle not subject to interference effects. From a con-sideration of experimental and theoretical data, the variation of C_{D_N} was estimated by adding the drag coefficients of a parabolic nose and a boattail from two different models (from reference 6) and the drag coef-ficient of a cylindrical section having a friction coefficient of 0.002. A comparison of the nacelle and the resulting reference body is shown in figure 2(a). The curve for the isolated nacelle drag is believed to be of sufficient accuracy to indicate the nacelle interference effects.

In order to compare the incremental nacelle drags, a composite chart for the four symmetrical positions tested is shown in figure 7(a). For the nacelles mounted symmetrically, a large difference in the drag exists between the forward and rearward positions. The values of the drag of the rear positions F and G are from 20 to 50 percent lower than the values of the drag of the forward positions D and E. It may be seen in fig-ure 7(a) that regions of favorable wing-nacelle-body interference are indicated below approximately $M = 0.93$.

Curves showing the incremental nacelle drag coefficients for the three underslung nacelle positions are presented in figure 7(b). The underslung positions experience no unfavorable interference effects up to approximately $M = 0.93$, which is comparable to results found for the symmetrical positions. The drag of the underslung nacelles is generally higher than the drag of symmetrically mounted nacelles. There is a very abrupt rise in the drag of the underslung nacelles starting at approxi-mately $M = 0.93$ and reaching a maximum at $M = 0.98$. The values of the drag of the symmetrical nacelles shown in figure 7(a) rise to a peak at a higher Mach number near $M = 1.01$. The 76-percent location, curve J, has the highest drag of the underslung as well as the symmetrical positions.

Figures 7(a) and 7(b) emphasize that the existence of unfavorable interference effects is most pronounced at a Mach number near $M = 1.0$ for the configuration tested. The unfavorable interference becomes less for Mach numbers less than or greater than $M = 1.0$. At a Mach number

.of 1.0 the increase in nacelle drag coefficient due to unfavorable inter-
ference varies from 85 percent to 285 percent of the drag coefficient
estimated for the isolated nacelle.

In general, it may be seen that the addition of nacelles on the wing
at the 40-percent-semispan station, independent of location, reduces the
drag rise Mach number by 0.03 to 0.07.

The variation of nacelle base-pressure coefficient for model J with
the underslung nacelle position, which has the most unfavorable inter-
ference drag, is presented for the test Mach number range in figure 8.
The accuracy of the base-pressure coefficient varies from ±0.038 at sub-
sonic speeds to ±0.013 at supersonic speeds. A pressure greater than
atmospheric acted on the nacelle base up to $M = 0.98$. The gradual
increase and sudden drop in base pressure at $M = 0.98$ may indicate
the movement of a shock wave to the rear of the nacelle base. The drag
resulting from this base pressure is shown in the lower part of fig-
ure 6(f). From the magnitude of the base-drag coefficients, it is
apparent that the base drag had little effect on the nacelle-plus-
interference drag at supersonic speeds; however, the positive base pres-
sure may contribute appreciably to reducing the nacelle drag at high
subsonic speeds.

In order to study more generally the effect of nacelle position on
the incremental nacelle drag, a cross plot of figure 7 for six Mach
numbers is presented in figures 9(a) to 9(f). Each figure shows the
nacelle-plus-interference drag coefficient for both underslung and sym-
metrical positions with varying chordwise location of the nacelle. The
lengths e and c defined in figure 2 are measured along the nacelle
center line at 40 percent of the wing semispan. The level of drag
expected, if there were no interference, is shown as a dash line called
"Isolated nacelle."

Figure 9(a) shows that at a Mach number of 0.9 the underslung posi-
tions have low drag coefficients which compare favorably with the sym-
metrical locations despite the fact that there were acute angles between
the wing and nacelle due to the absence of filleting on any of the models.
The indication that favorable interference effects exist for the 35-percent
symmetrical position is supported by similar favorable effects found in
reference 7. At $M = 0.95$ (fig. 9(b)) the 35-percent symmetrical posi-
tion has the lowest drag coefficient. The variations in drag at $M = 1.0$
are shown in figure 9(c). The trend shows that the symmetrical positions
have lower drag than the corresponding underslung positions. Nacelles
at the 35- and 50-percent symmetrical positions have approximately equal
drag, but a large rise in drag is experienced in moving the nacelle for-
ward from the 50- to the 76-percent station. The same general trends
are shown at $M = 1.05$ (fig. 9(d)) and $M = 1.15$ (fig. 9(e)). The
76-percent position has the largest drag increment for all locations

tested. The highest test Mach number of 1.25 (shown in fig. 9(f)) indicates that no unfavorable interference was present for the 35-percent and 50-percent locations.

From these tests it is apparent that the drag increment associated with adding nacelles to a wing-body combination is largely dependent upon the nacelle location.

CONCLUSIONS

Swept-wing-nacelle interference effects have been obtained experimentally by transonic flight tests at zero lift. Underslung and symmetrically mounted solid nacelles were varied in a direction parallel to the free stream along the wing chord at the 40-percent station of a 45° sweptback wing. The following effects were noted:

1. No unfavorable interference effects were evident for either underslung or symmetrical nacelles at Mach numbers between 0.80 and 0.93.

2. The highest nacelle drag coefficients measured throughout the test Mach number range occurred near M = 1.0. At this Mach number the nacelle drag coefficients were from 85 percent to 285 percent higher than the drag coefficient estimated for the nacelle without interference.

3. Nacelles mounted symmetrically on the wing generally had lower drag coefficients than nacelles located in underslung positions at Mach numbers from 0.95 to 1.20.

4. The symmetrically mounted nacelles located at rearward positions at the 35- and 50-percent-chord stations gave the lowest drag.

5. The highest drag for the underslung nacelle positions was found to be the 76-percent-chord station, and moving the nacelle forward or rearward from this position lowered the drag.

6. The addition of nacelles on the wings of the models, independent of their chordwise location at 40 percent of the semispan, reduced the Mach number at which the transonic drag rise of the total configuration occurred by 0.03 to 0.07.

Langley Aeronautical Laboratory
        National Advisory Committee for Aeronautics
                Langley Air Force Base, Va.

REFERENCES

1. Thompson, Jim Rogers: Measurements of the Drag and Pressure Distri-
   bution on a Body of Revolution throughout Transition from Subsonic
   to Supersonic Speeds. NACA RM L9J27, 1950.

2. Spreemann, Kenneth P., Morrison, William D., Jr., and Pasteur,
   Thomas B., Jr.: Aerodynamic Characteristics of a Wing with Quarter-
   Chord Line Swept Back 45°, Aspect Ratio 6, Taper Ratio 0.6, and
   NACA 65A009 Airfoil Section. Transonic-Bump Method. NACA RM L50B03a,
   1950.

3. Baals, Donald D., Smith, Norman F., and Wright, John B.: The Develop-
   ment and Application of High-Critical-Speed Nose Inlets. NACA
   Rep. 920, 1948.

4. Abbott, Ira H.: Fuselage-Drag Tests in the Variable-Density Wind
   Tunnel: Streamline Bodies of Revolution, Fineness Ratio of 5.
   NACA TN 614, 1937.

5. Dannenberg, Robert E.: The Development of Jet-Engine Nacelles for a
   High-Speed Bomber Design. NACA RM A7D10, 1947.

6. Hart, Roger G., and Katz, Ellis R.: Flight Investigations at High-
   Subsonic, Transonic, and Supersonic Speeds to Determine Zero-Lift
   Drag of Fin-Stabilized Bodies of Revolution Having Fineness Ratios
   of 12.5, 8.91, and 6.04 and Varying Positions of Maximum Diameter.
   NACA RM L9I30, 1949.

7. Welsh, Clement J., and Morrow, John D.: Effect of Wing-Tank Location
   on the Drag and Trim of a Swept-Wing Model as Measured in Flight at
   Transonic Speeds. NACA RM L50A19, 1950.

TABLE I

FUSELAGE COORDINATES

x (in.)	y (in.)
0	0
.4	.185
.6	.238
1.0	.342
2.0	.578
4.0	.964
6.0	1.290
8.0	1.577
12.0	2.074
16.0	2.472
20.0	2.772
24.0	2.993
28.0	3.146
32.0	3.250
36.0	3.314
40.0	3.334
44.0	3.304
48.0	3.219
52.0	3.037
56.0	2.849
60.0	2.661
64.0	2.474
66.7	2.347

NACA

TABLE II

COORDINATES OF THE NACA 65A009 AIRFOIL

x/c (percent)	y/c (percent)
0	0
.5	.688
.75	.835
1.25	1.065
2.5	1.460
5.0	1.964
7.5	2.385
10.0	2.736
15.0	3.292
20.0	3.714
25.0	4.036
30.0	4.268
35.0	4.421
40.0	4.495
45.0	4.485
50.0	4.377
55.0	4.169
60.0	3.874
65.0	3.509
70.0	3.089
75.0	2.620
80.0	2.117
85.0	1.594
90.0	1.069
95.0	.544
100.0	.019

TABLE III

COORDINATES FOR SOLID NACELLE

x (in.)	y (in.)
0	0
.100	.070
.330	.169
.830	.336
1.330	.489
1.830	.622
2.330	.747
2.580	.800
2.958	.876
3.585	.974
4.840	1.105
6.095	1.190
7.350	1.240
8.605	1.255
16.830	1.255
17.872	1.237
18.913	1.195
19.955	1.127
20.996	1.029
22.038	.909
23.079	.768
24.121	.616
24.250	.598
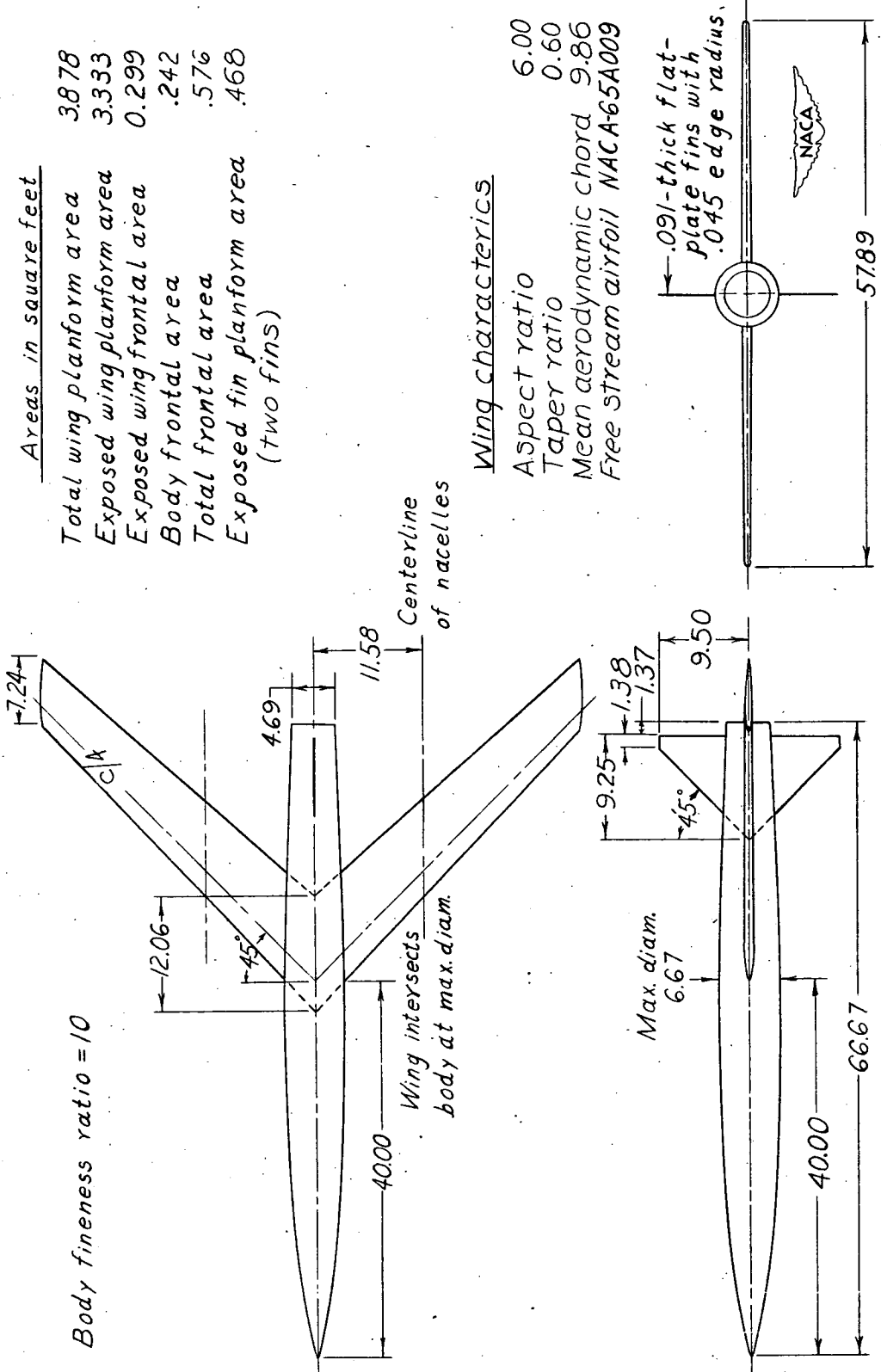
Areas in square feet

Total wing planform area   3.878
Exposed wing planform area 3.333
Exposed wing frontal area   0.299
Body frontal area   .242
Total frontal area   .576
Exposed fin planform area   .468
      (two fins)

Wing characterics

Aspect ratio   6.00
Taper ratio   0.60
Mean aerodynamic chord   9.86
Free stream airfoil NACA-65A009

.091-thick flat-
plate fins with
.045 edge radius.

NACA

57.89

Centerline
of nacelles

11.58

4.69

7.24

C/4

12.06

45°

4000

Wing intersects
body at max.diam.

Body fineness ratio = 10

1.38
1.37

9.25

9.50

45°

Max. diam.
6.67

66.67

40.00

Figure 1.- General arrangement and dimensions of test model. All
dimensions are in inches.

Nose plug | NACA 1-50-250 nacelle inlet (solid) | Cylindrical midsection | NACA III afterbody

Nacelle frontal area = 0.034 sq ft
Nacelle fineness ratio = 9.66
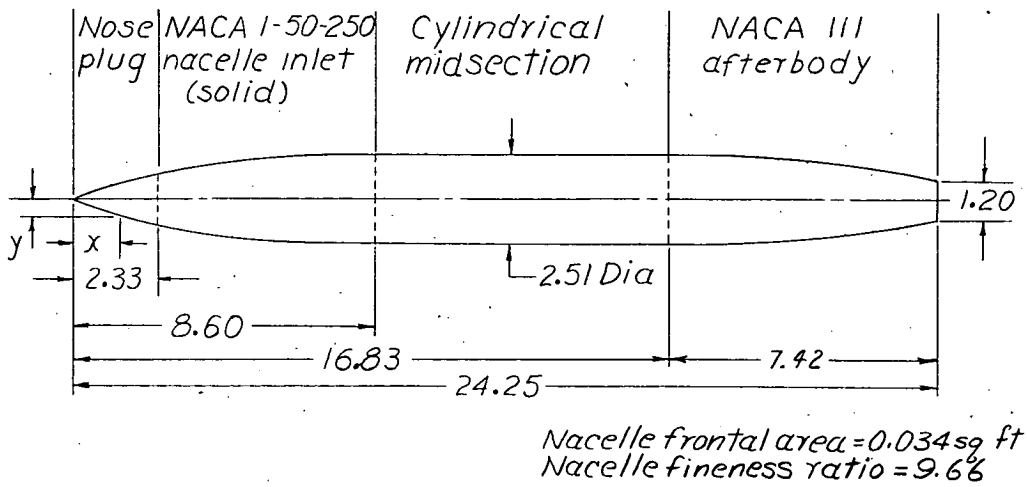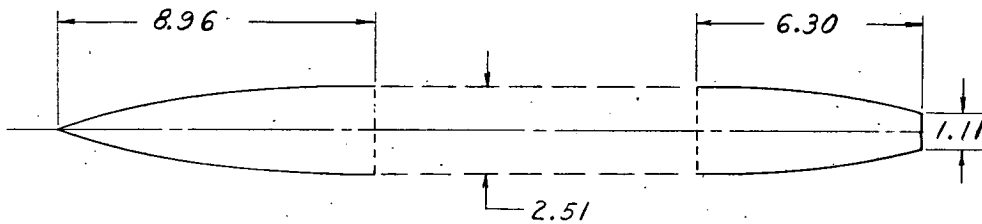
Nacelle

Isolated Nacelle
Drag reference body

(a) Comparison of nacelle and isolated nacelle.

Figure 2.- Dimensions and arrangement of nacelles. All dimensions are in inches.
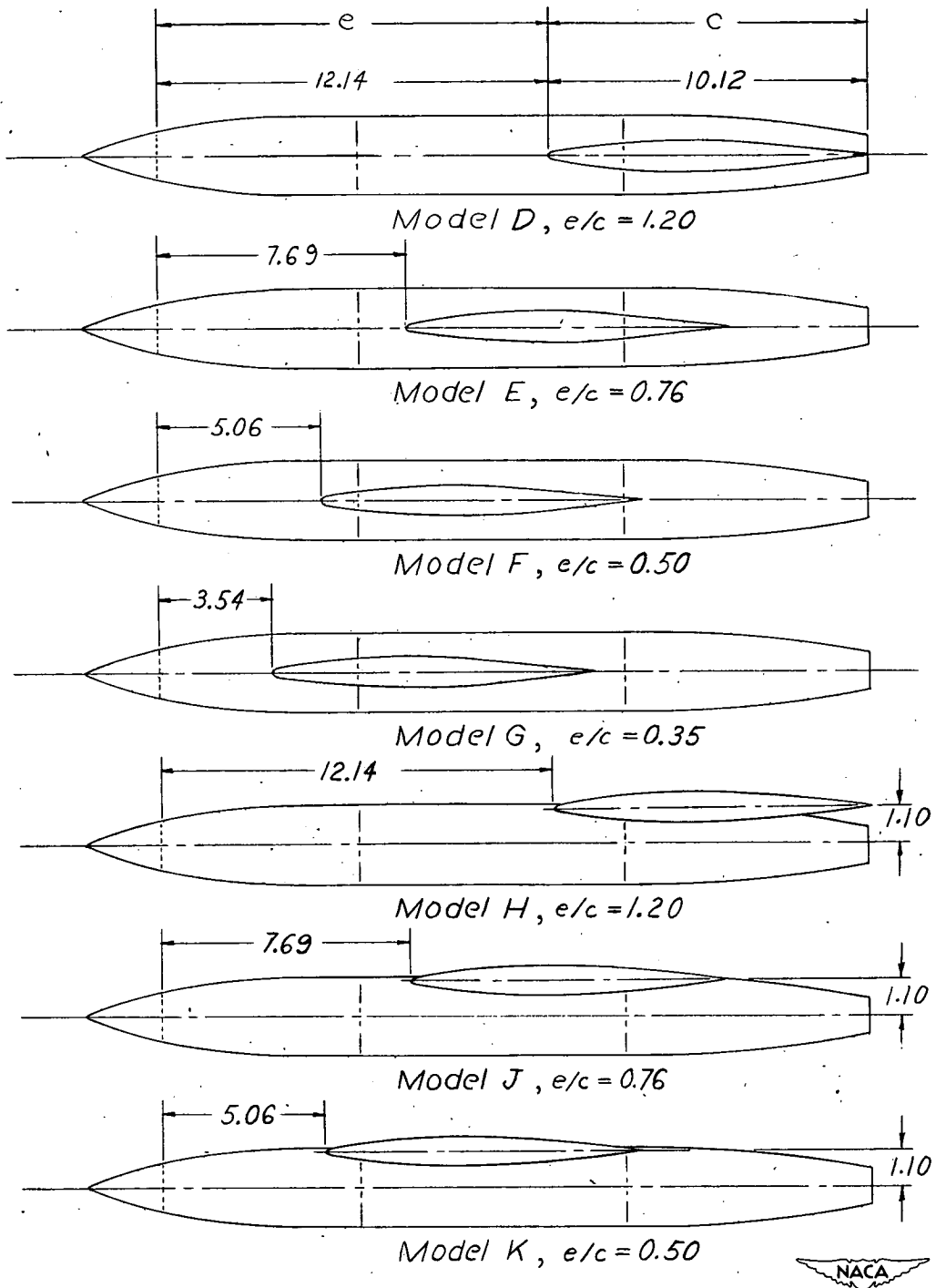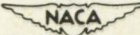
(b) Nacelle location on wing chord at 40 percent semispan.

Figure 2.- Concluded.

Models A, B, C   L-64912

(a) Test model without nacelles. Method of launching and boosting of
models at test area.

Figure 3.- General arrangement of test models.

Page intentionally left blank
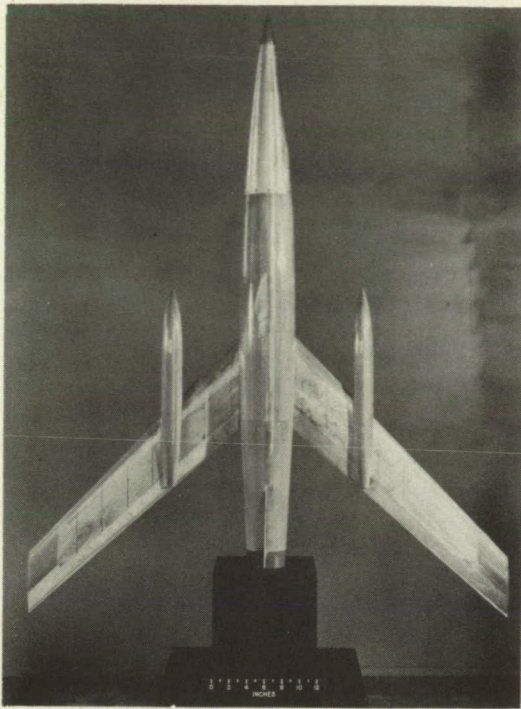
Model D, $\frac{e}{c} = 1.20$.
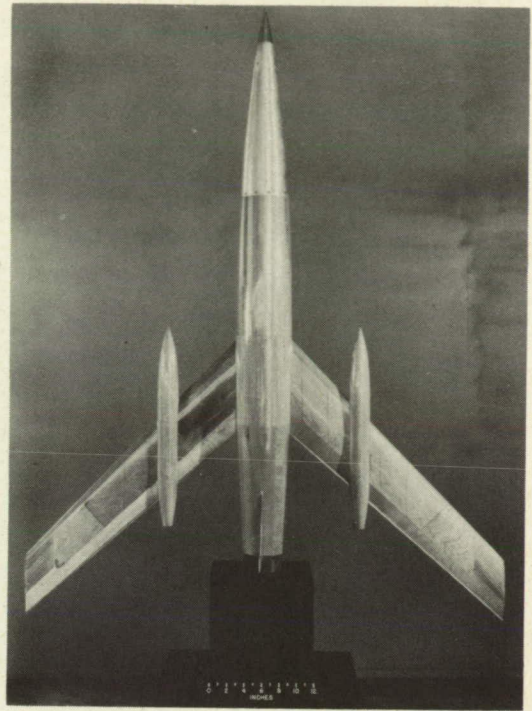
Model E, $\frac{e}{c} = 0.76$.
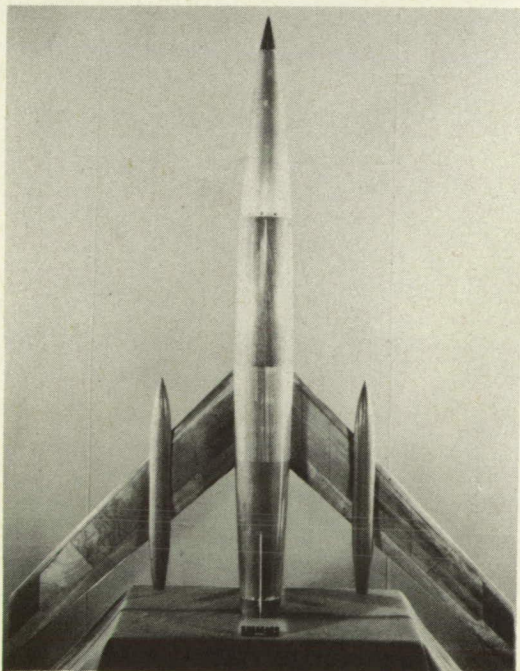
Model F, $\frac{e}{c} = 0.50$.
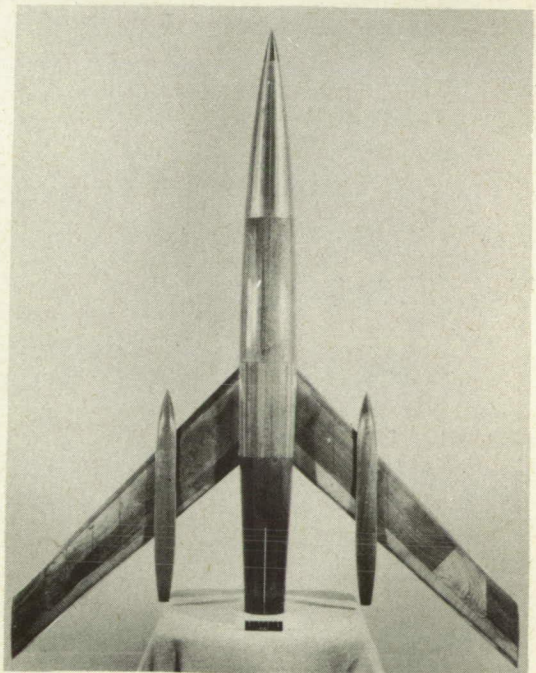
Model G, $\frac{e}{c} = 0.35$.

(b) Models with symmetrically mounted nacelles.
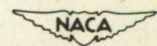
L-64913

Figure 3.- Continued.

Page intentionally left blank
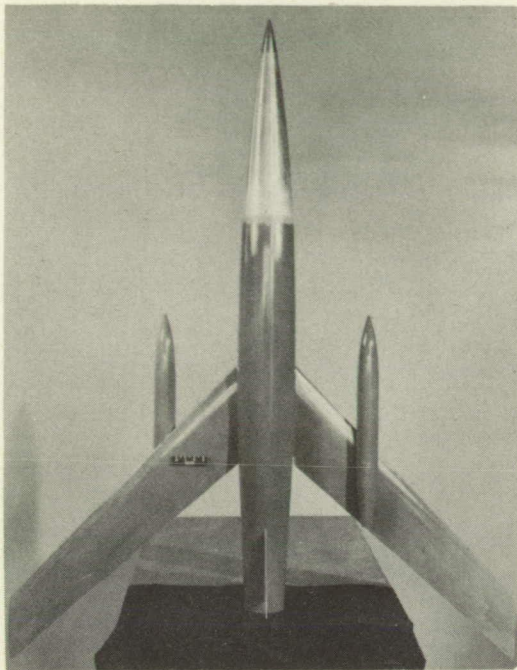
Model H, $\frac{e}{c} = 1.20$.
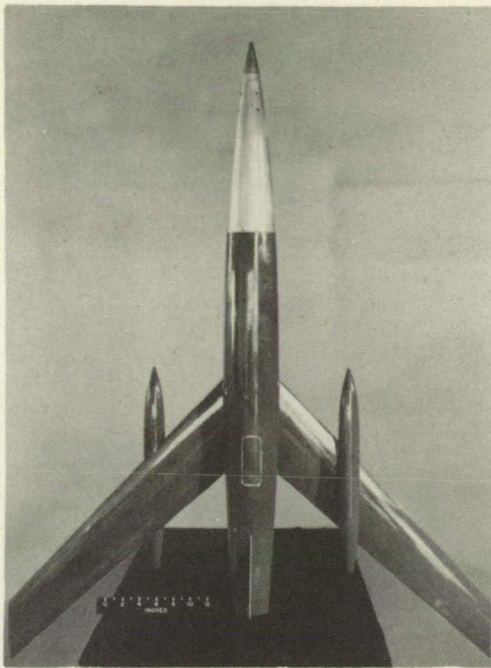
Model J, $\frac{e}{c} = 0.76$.
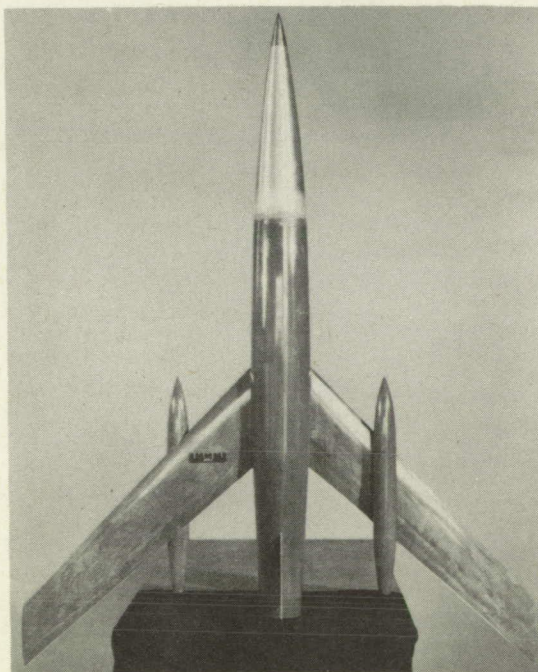
Model K, $\frac{e}{c} = 0.50$.

(c) Models with underslung nacelles.

L-64914

Figure 3.- Concluded.

Page intentionally left blank
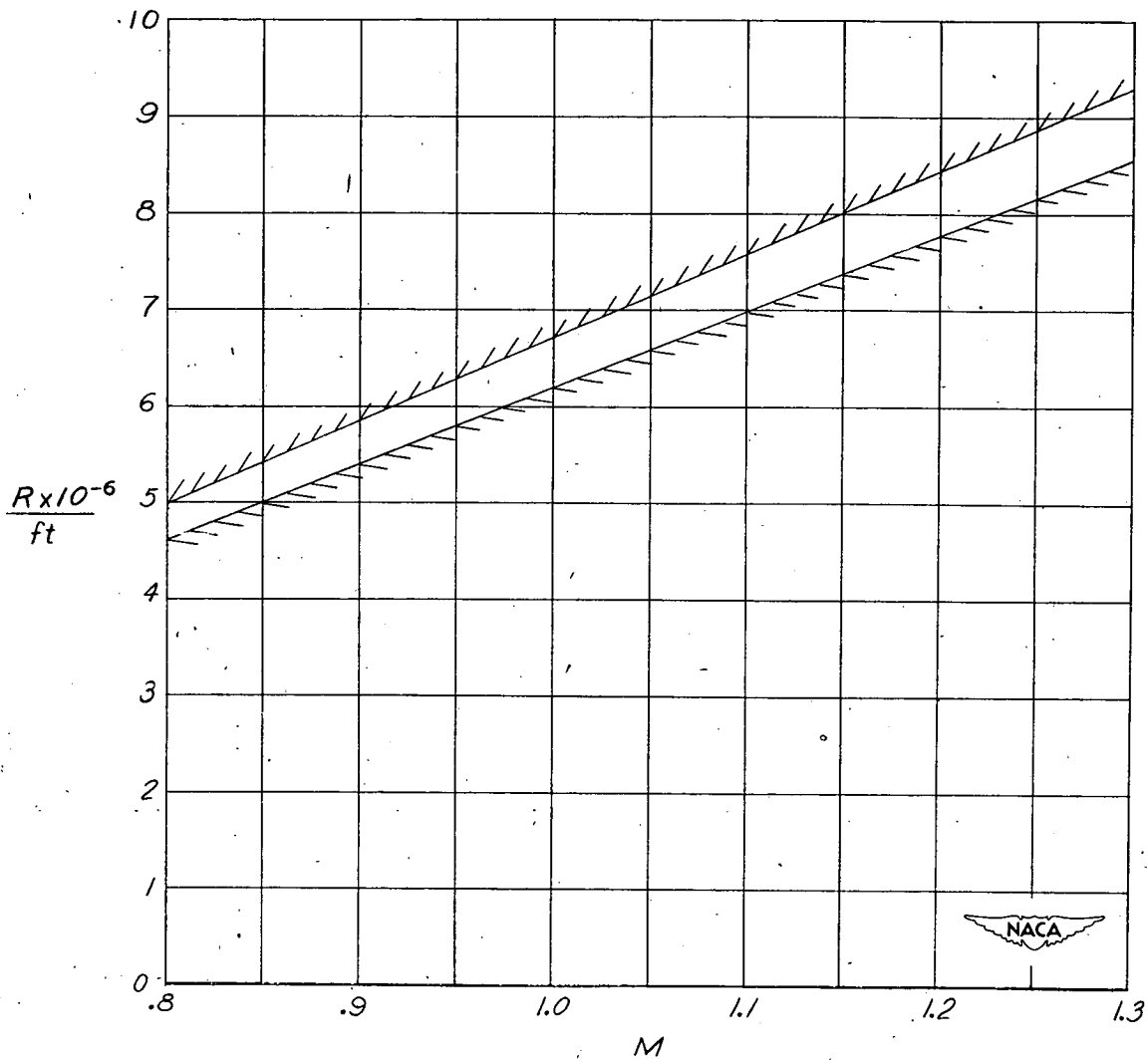
Figure 4.- Variation of Reynolds number range with Mach number for models tested.
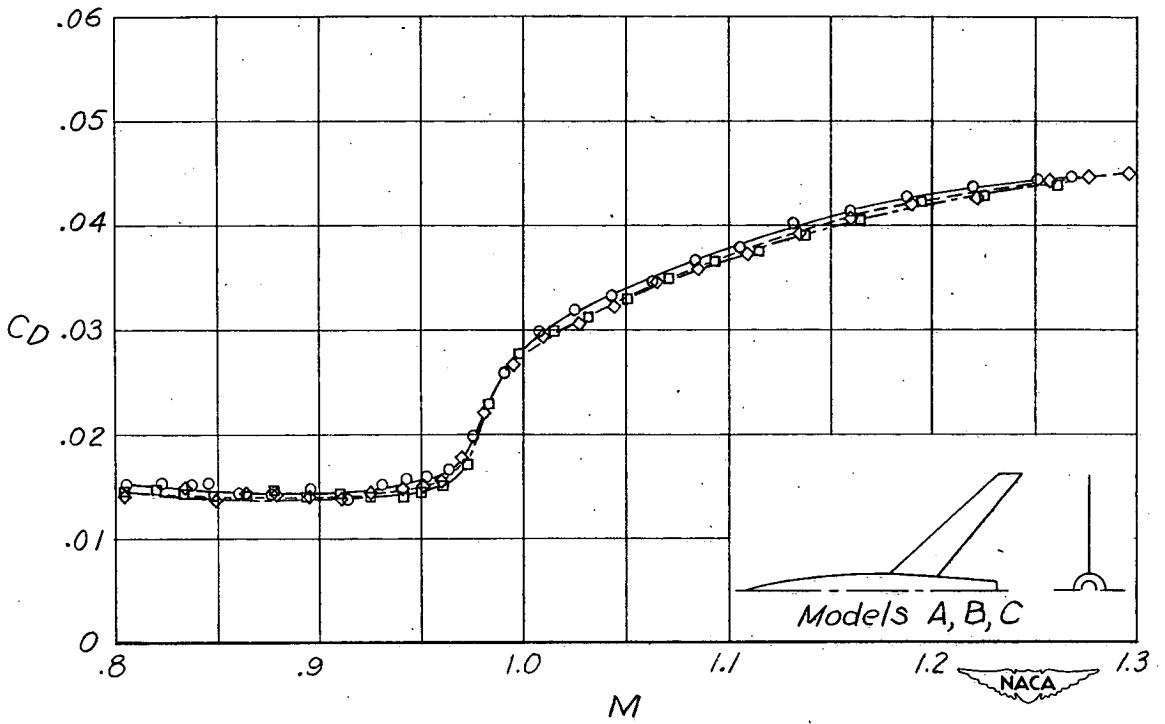
Figure 5.- Variation of drag coefficient for models without nacelles.
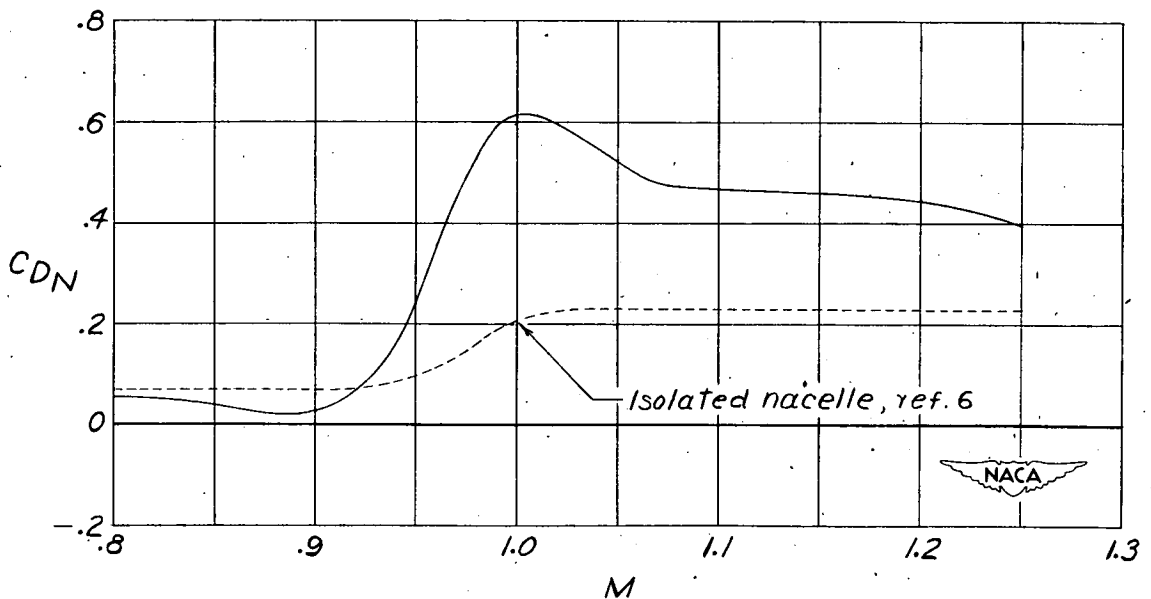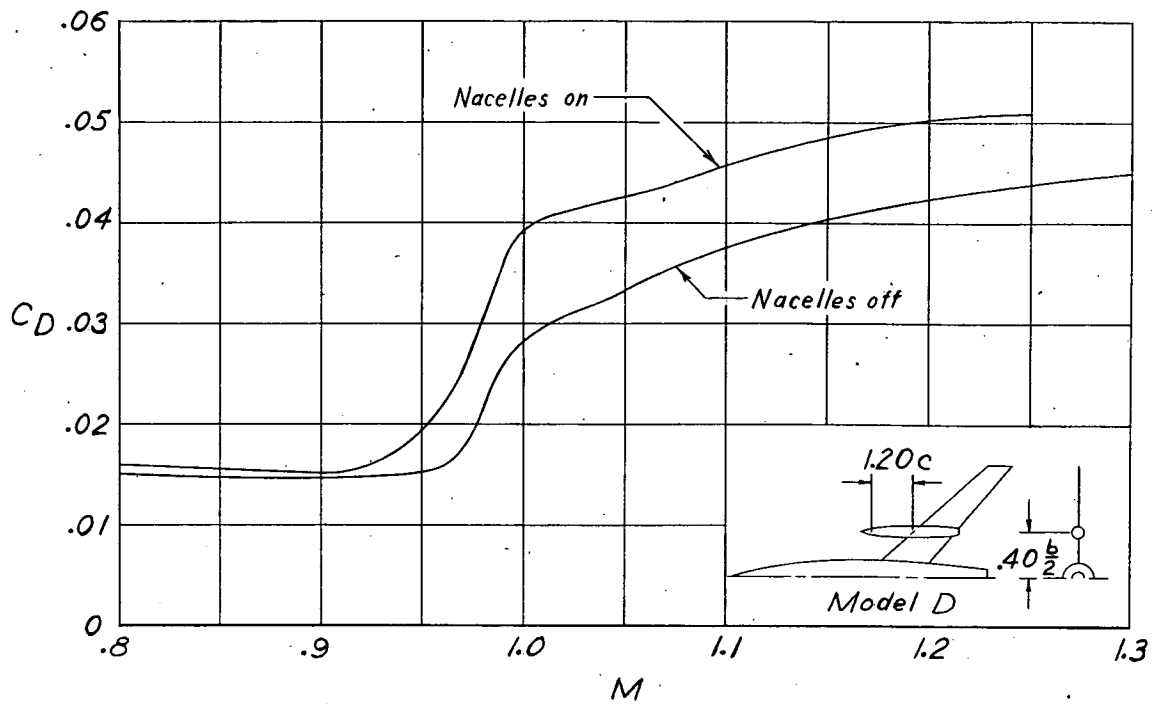
(a) Symmetrically mounted nacelles at 1.20c.

Figure 6.- Variations of total drag, wing-body drag, and nacelle drag
   coefficients with Mach number for nacelles located at 40 percent of
   the wing semispan.
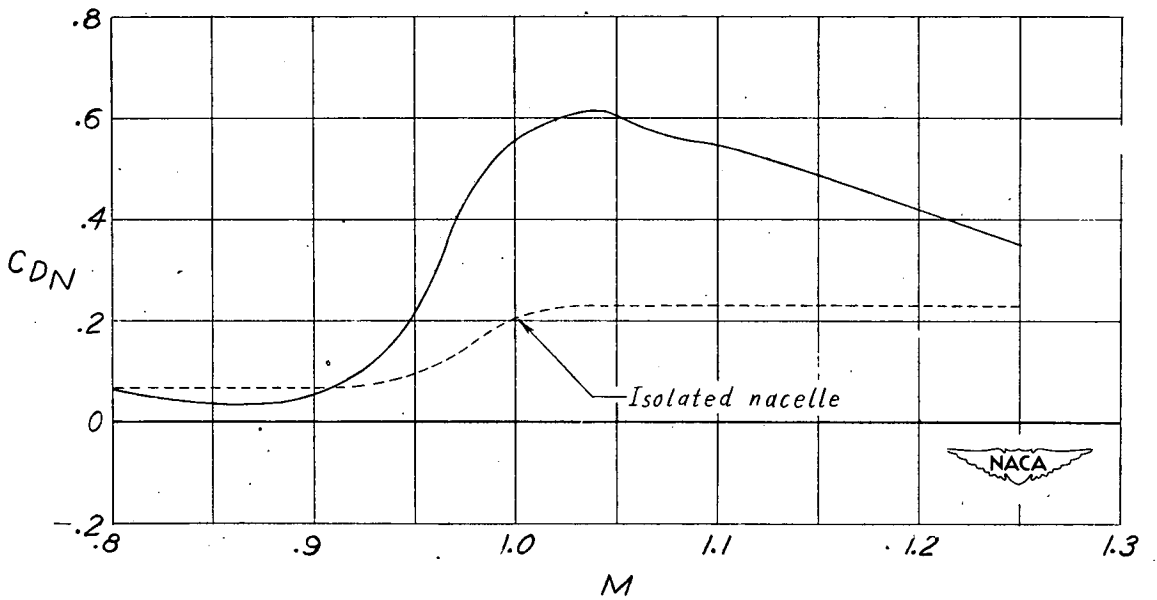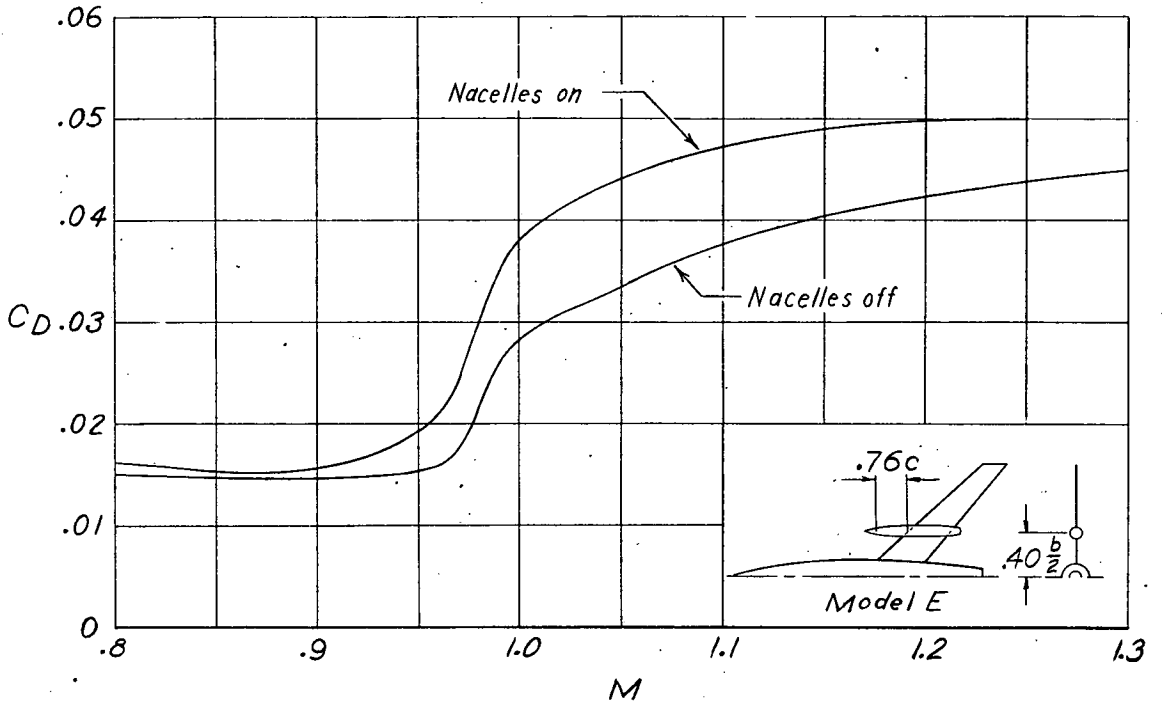
(b) Symmetrically mounted nacelles at 0.76c.

Figure 6.- Continued.
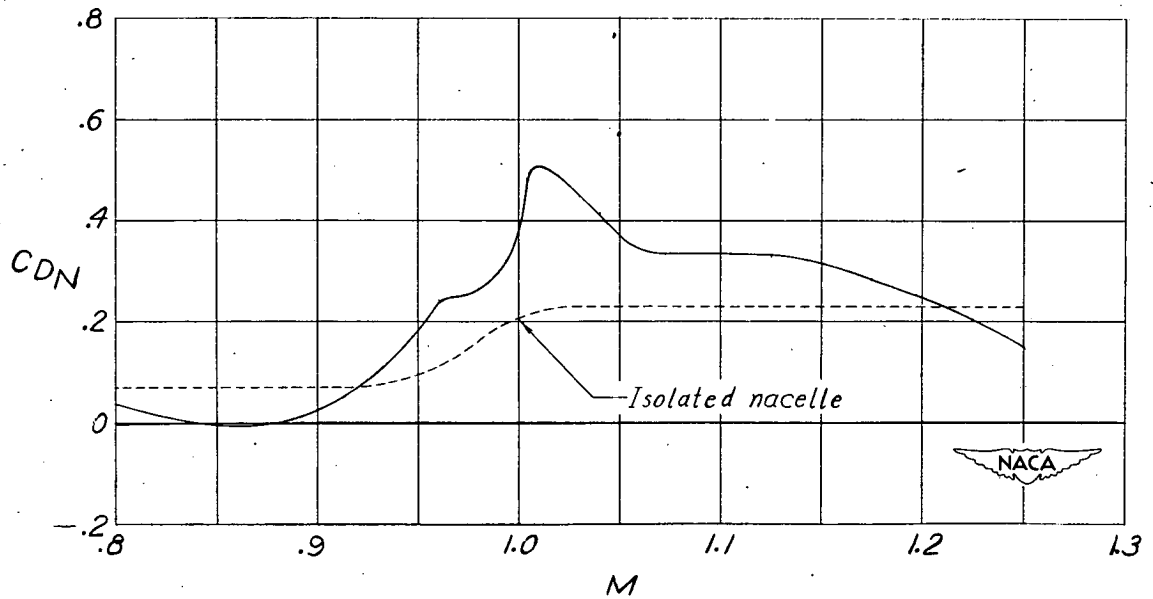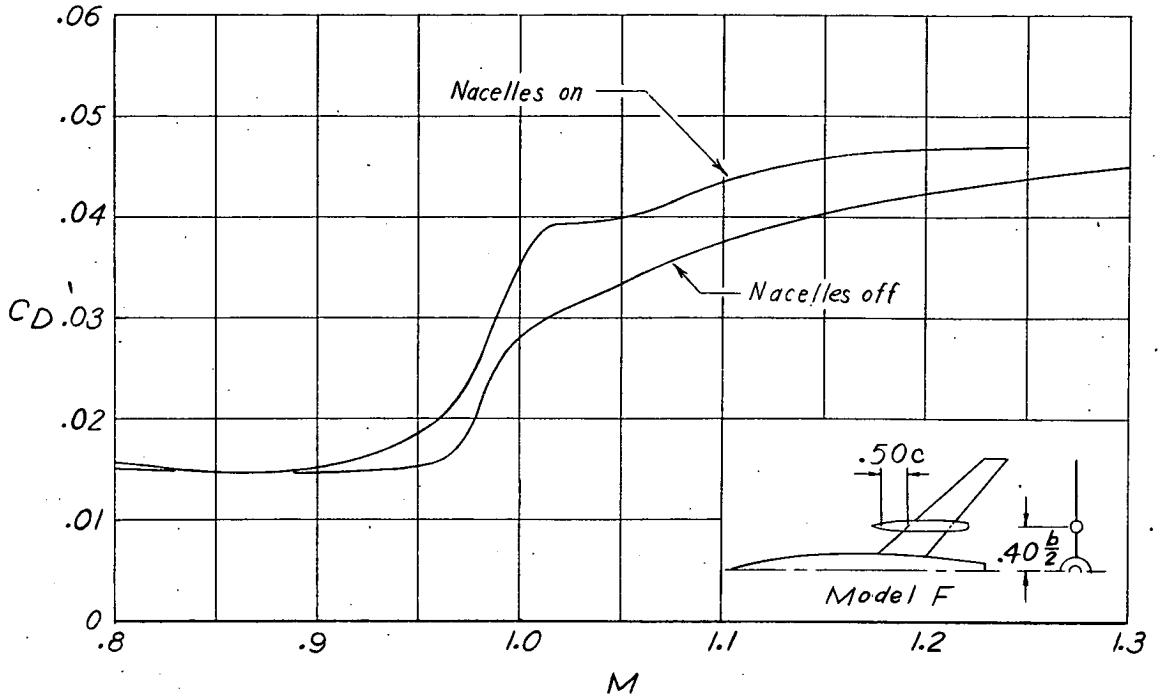
(c) Symmetrically mounted nacelles at 0.50c.

Figure 6.- Continued.
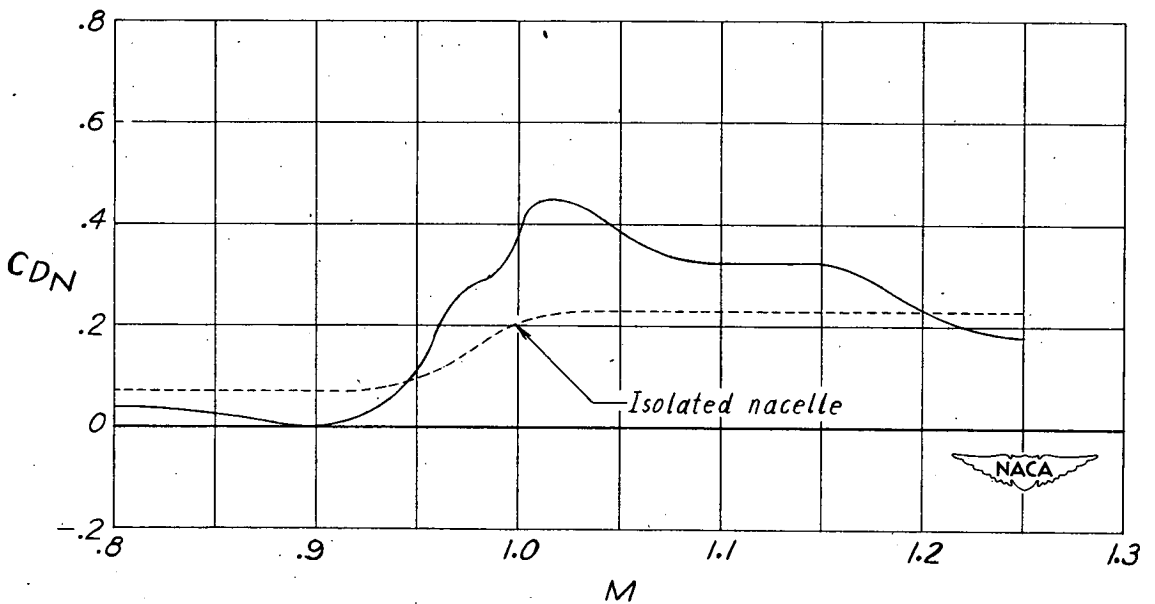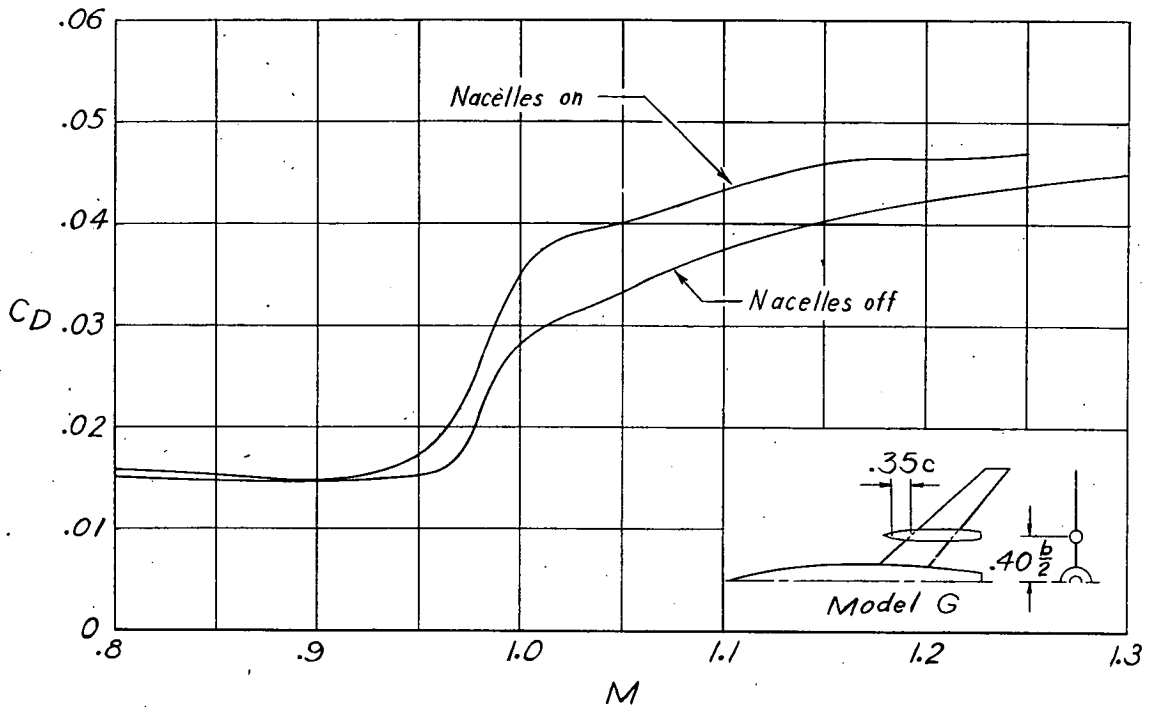
(d) Symmetrically mounted nacelles at 0.35c.

Figure 6.- Continued.
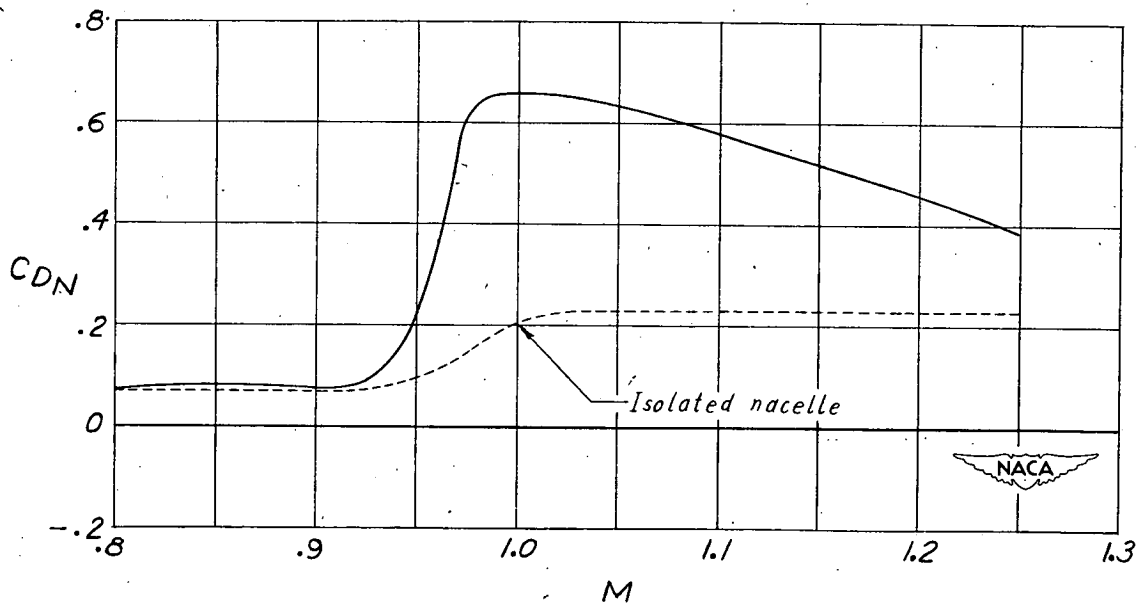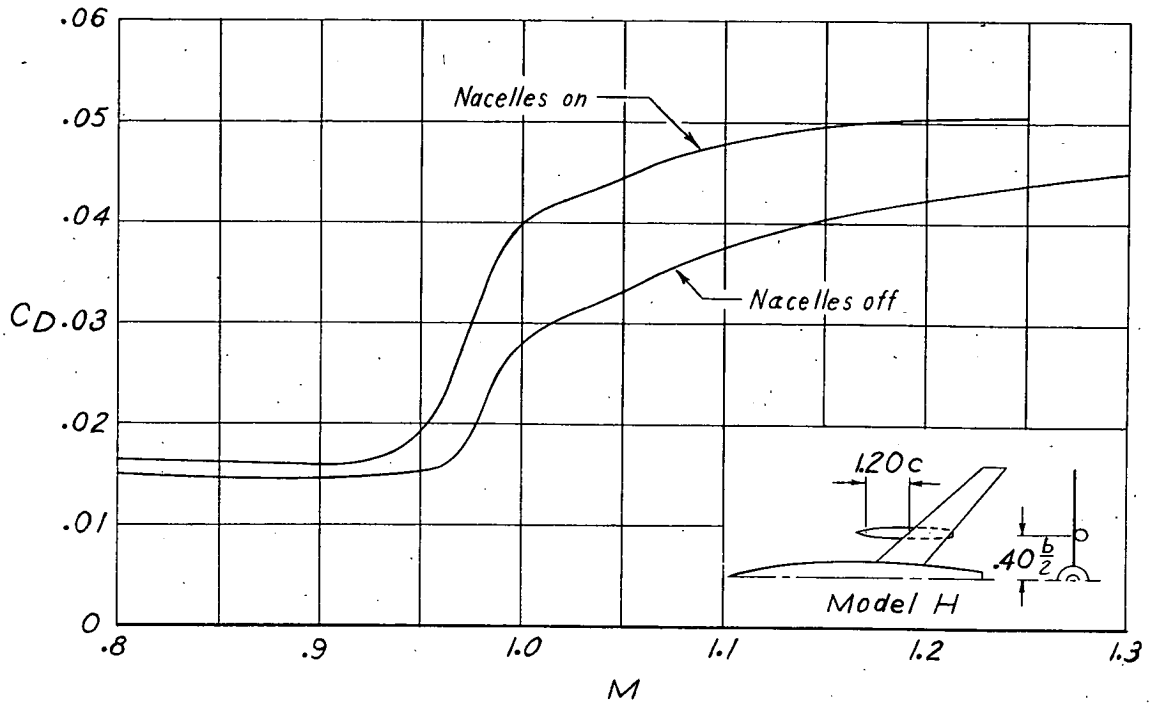
(e) Underslung nacelles at 1.20c.

Figure 6.- Continued.
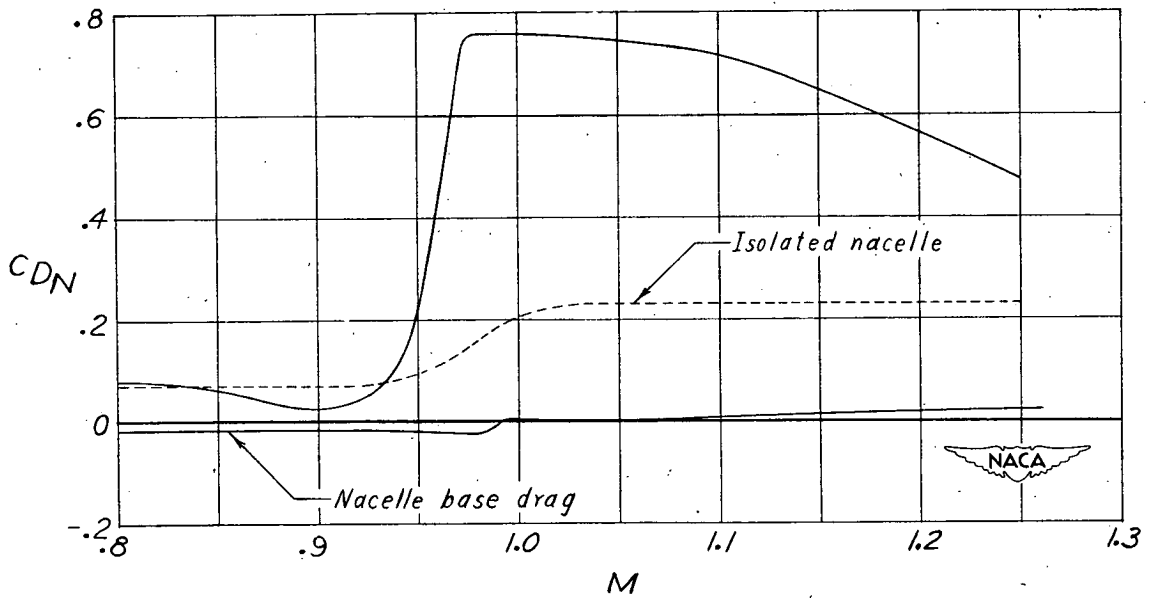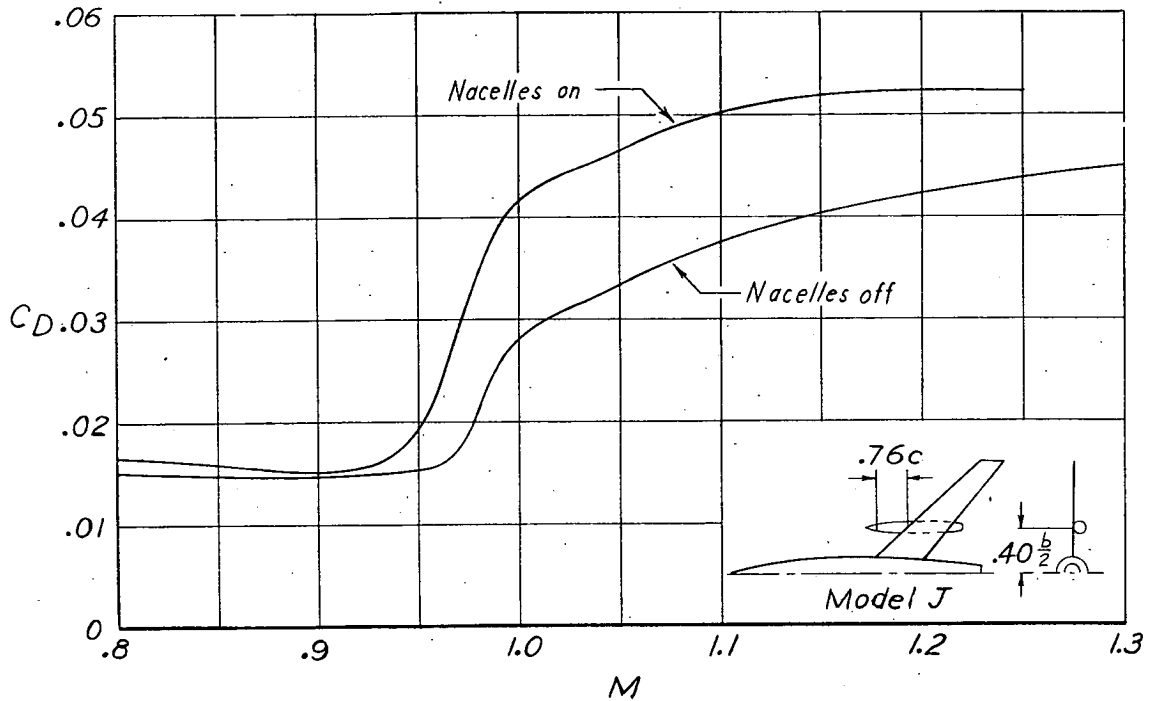
(f) Underslung nacelles at 0.76c.

Figure 6.- Continued.
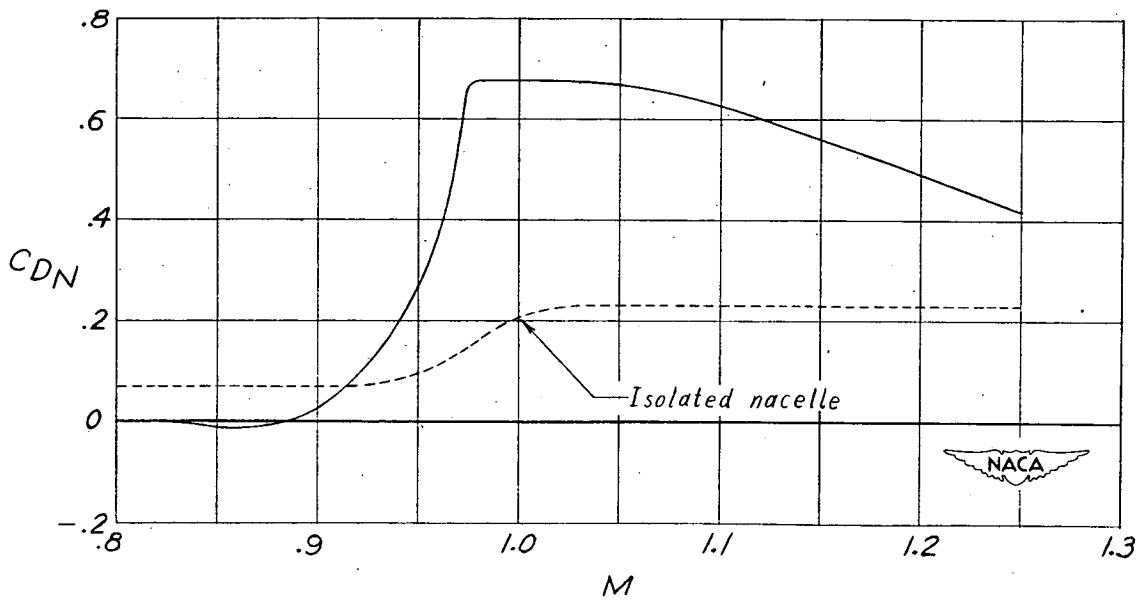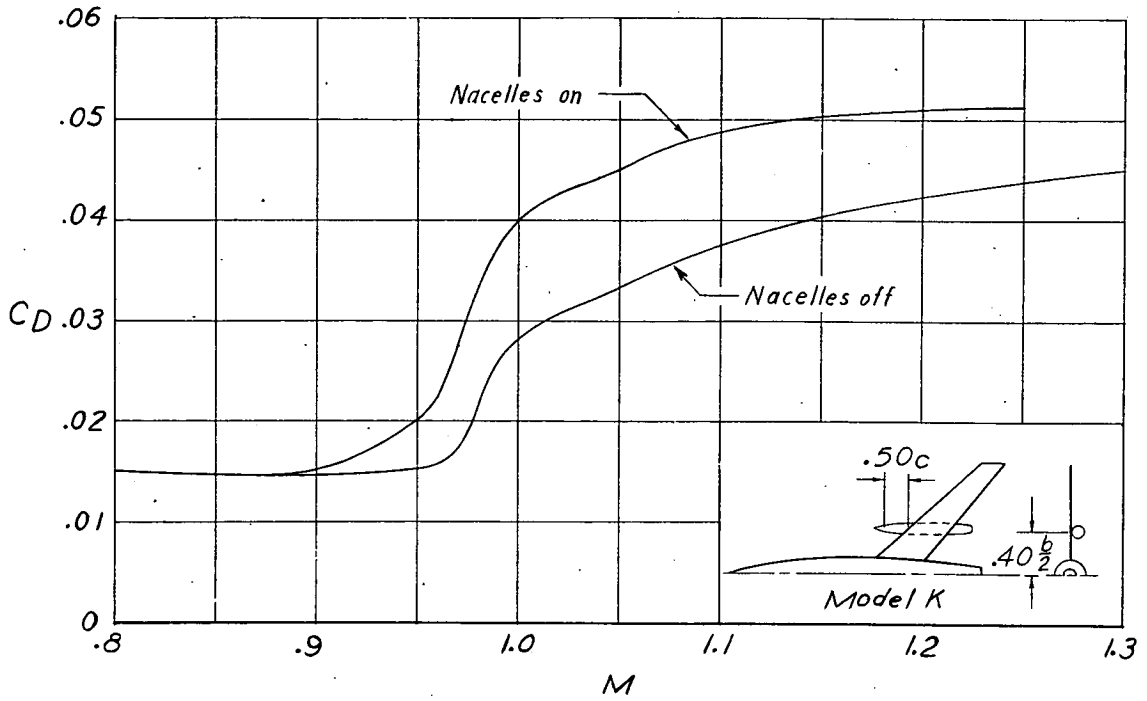
(g) Underslung nacelles at 0.50c.

Figure 6.- Concluded.
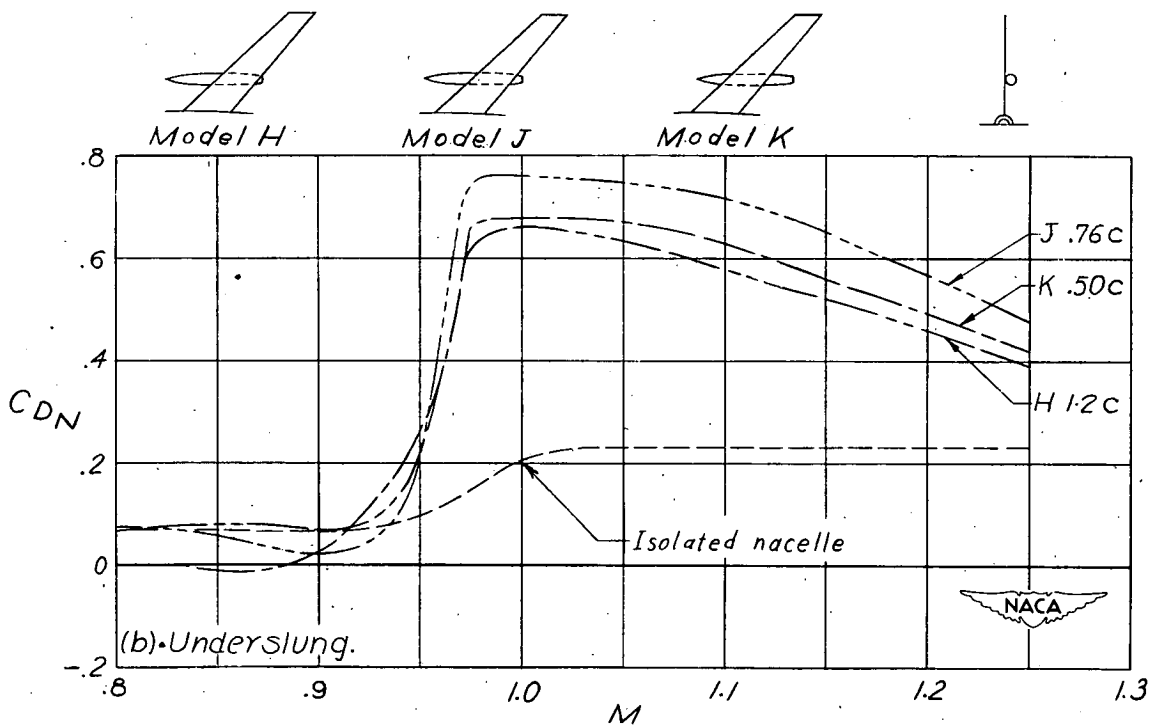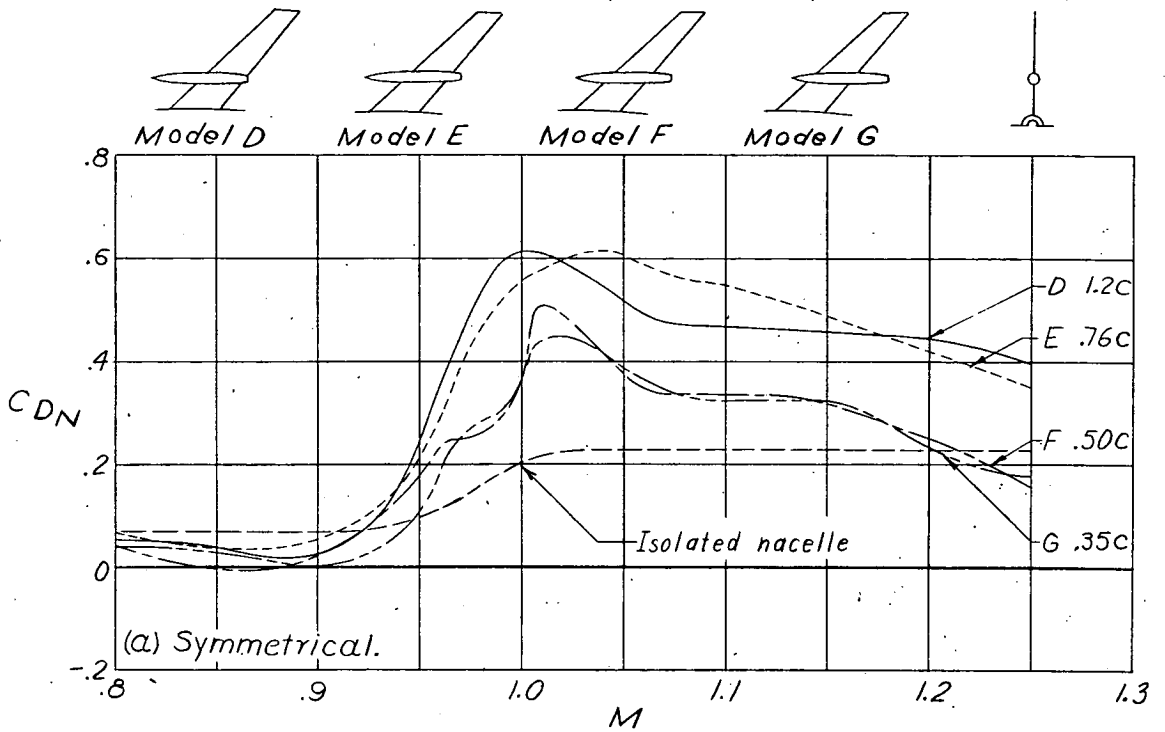
Figure 7.- Variations of nacelle drag coefficients with Mach number for nacelles mounted in various chordwise locations and in symmetrical and underslung positions.
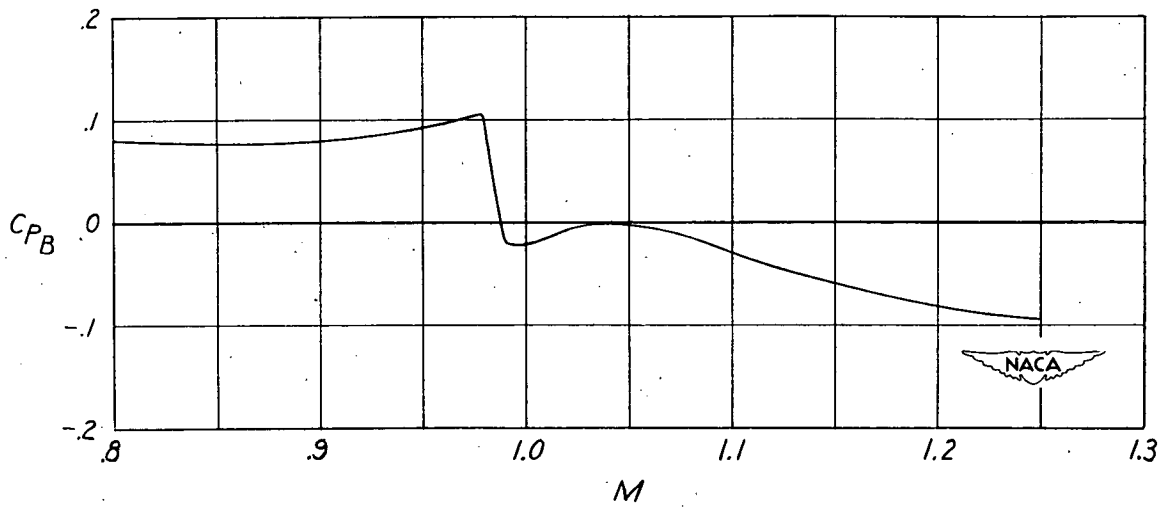
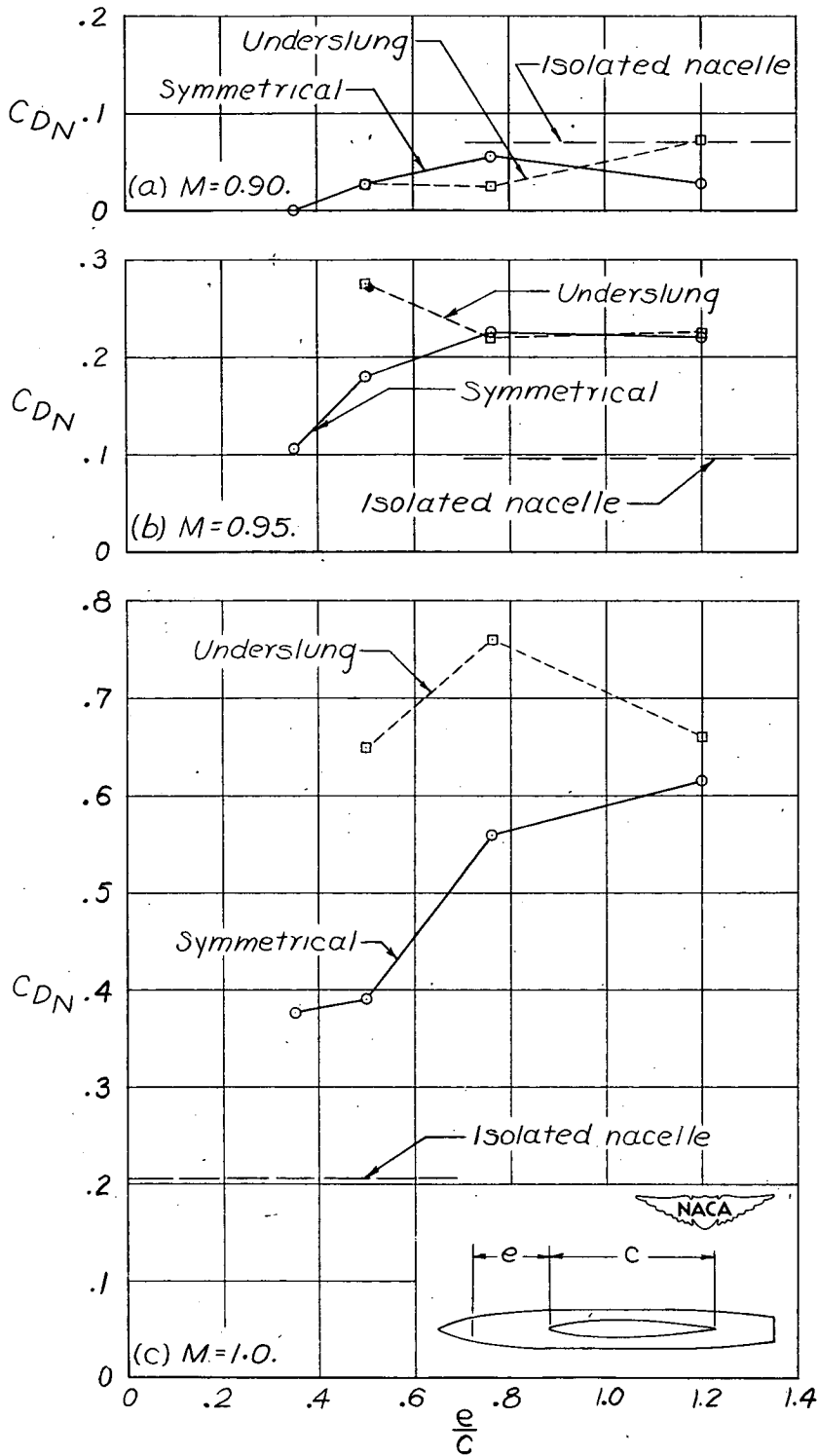Figure 8.- Variation of nacelle base-pressure coefficient with Mach number for model J.

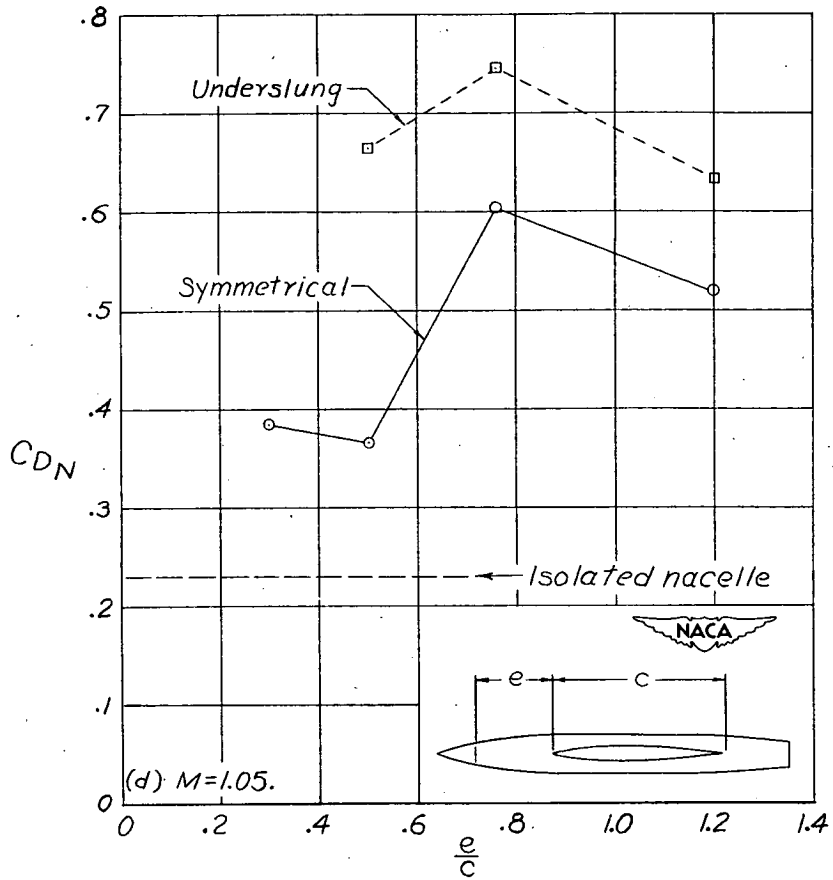Figure 9.- Variations of nacelle drag coefficient with chordwise location of nacelles in symmetrical and underslung positions for various Mach numbers.
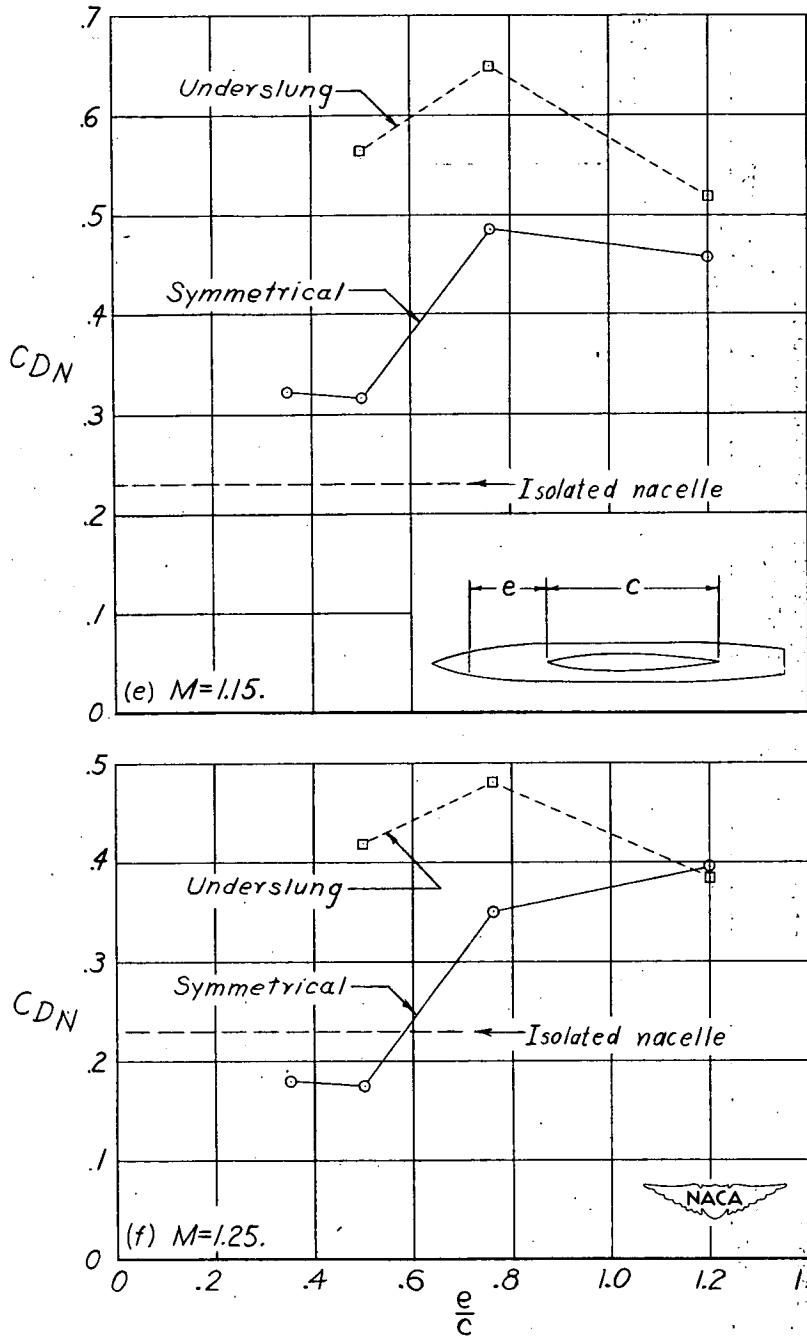
Figure 9.- Continued.

Figure 9.- Concluded.